

1 A Global Ozone Profile Climatology for Satellite Retrieval
2 Algorithms Based on Aura MLS Measurements and the
3 MERRA-2 GMI Simulation
4
5

6 Jerald R. Ziemke^{1,2}, Gordon J. Labow³, Natalya A. Kramarova¹, Richard D. McPeters¹, Pawan
7 K. Bhartia¹, Luke D. Oman¹, Stacey M. Frith³, and David P. Haffner³
8

9 ¹NASA Goddard Space Flight Center, Greenbelt, Maryland, USA

10 ²Morgan State University, Baltimore, Maryland, USA

11 ³SSAI, Lanham, Maryland, USA
12

13 **Abstract.** A new atmospheric ozone profile climatology has been constructed by combining
14 daytime ozone profiles from the Aura Microwave Limb Sounder (MLS) and Modern-Era
15 Retrospective Analysis for Research Applications version 2 (MERRA2) Global Modeling
16 Initiative (GMI) model simulation (M2GMI). The MLS and M2GMI ozone profiles are merged
17 between 13 and 17 km (~159 and 88 hPa) with MLS used for stratospheric and GMI for
18 primarily tropospheric levels. The time record for profiles from MLS and GMI is August 2004-
19 December 2016. The derived seasonal climatology consists of monthly zonal-mean ozone
20 profiles in 5-degree latitude bands from 90°S-90°N covering altitudes (in Z* log-pressure
21 altitude) from zero to 80 km in 1 km increments. This climatology can be used as a priori
22 information in satellite ozone retrievals, in atmospheric radiative transfer studies, and as a
23 baseline to compare with other measured or model-simulated ozone. The MLS/GMI seasonal
24 climatology shows a number of improvements compared to previous ozone profile climatologies
25 based on MLS and ozonesonde measurements. These improvements are attributed mostly to
26 continuous daily global coverage of GMI tropospheric ozone compared to sparse regional
27 measurements from sondes. In addition to the seasonal climatology, we also derive an additive
28 climatology to account for inter-annual variability in stratospheric zonal-mean ozone profiles
29 which is based on a rotated empirical orthogonal function (REOF) analysis of Aura MLS ozone

30 profiles. This REOF climatology starts in 1970 and captures most of the inter-annual variability
31 in global stratospheric ozone including Quasi-Biennial Oscillation (QBO) signatures.

32

33 **1. Introduction.**

34

35 McPeters and Labow (2012) (hereafter, ML) and Labow et al. (2015) combined ozone profile
36 data from ozonesondes and the Aura Microwave Limb Sounder (MLS) (Livesey et al., 2011) to
37 use as climatological a priori information for satellite retrievals of ozone. These ozone profile
38 climatologies were constructed by merging ozonesondes in the troposphere with satellite ozone
39 in the stratosphere/mesosphere. For the ML climatology the stratosphere/mesosphere portion of
40 the climatological ozone profiles was based on averaging MLS daytime and nighttime limb
41 measurements. The mix of daytime and nighttime measurements led to smearing of the ozone
42 diurnal cycle in the upper stratosphere and lower mesosphere.

43

44 The limited amount and sparse spatial coverage of ozonesonde data has led us to now use the
45 NASA Goddard Earth Observing System (GEOS) Global Modeling Initiative (GMI) model as a
46 substitute for the ozonesonde data in the lower atmosphere. The GMI model uses Modern-Era
47 Retrospective Analysis for Research Applications version 2 (MERRA2) meteorology. We refer
48 to this as the MERRA2 GMI (hereafter M2GMI) model.

49

50 We have generated a new ozone profile zonal-mean seasonal climatology (MLS/GMI) based on
51 combining MLS v4.2 and M2GMI ozone profiles which represents an improvement from our
52 previous sonde-satellite ozone climatologies including ML. The earlier climatologies were
53 binned in 10-degree latitude bands due mostly to the limited coverage of sondes. In contrast, the
54 new MLS/GMI ozone profile climatology has been binned to 5° latitude bands by taking
55 advantage of better spatial and temporal coverage of the model output. This new climatology
56 also extends to 80 km in altitude compared to 65 km in the previous climatologies. The new
57 MLS/GMI ozone profile climatology is provided for both volume mixing ratio (units ppmv) and
58 vertical column concentration (Dobson Units (DU) km⁻¹).

59

60 We also generated a new inter-annual ozone profile climatology based on MLS ozone, SBUV
61 total ozone, and rawinsonde wind data using a rotated empirical orthogonal function (REOF)
62 method. This REOF inter-annual climatology, just like the MLS/GMI seasonal climatology
63 includes monthly-zonal mean profile ozone concentration (units DU km⁻¹) within 5° latitude
64 bands and altitudes 0-80 km; however, the REOF climatology represents a long time-dependent
65 record beginning 1970 rather than a 12-month time record for the MLS/GMI climatology.

66
67 The application of the MLS/GMI seasonal climatology by itself or together with the REOF inter-
68 annual climatology as a priori enables more accurate profile and column ozone retrievals,
69 including improvements for inter-calibrating and merging independent satellite ozone
70 measurements such as for the SBUV Merged Ozone Dataset (MOD) (Frith et al., 2014). The
71 REOF climatology has recently been used to improve the calibration of long-record ozone
72 measurements from ground Umkehr instruments (I. Petropavlovskikh, personal communication,
73 2021) and from series of SBUV instruments. The REOF climatology has also recently been used
74 to improve SBUV ozone profile retrievals by adding inter-annual variability which nadir
75 instruments can not retrieve due to a coarse vertical resolution. These SBUV ozone profiles with
76 improved inter-annual variability can be used for the assimilated profile ozone records like one
77 from the Goddard Modeling and Assimilation Office (GMAO)(K. Wargan, personal
78 communication, 2021).

79
80 In the following sections we describe the data and GMI model output used in our analysis,
81 outline the methods used to construct the MLS/GMI seasonal climatology and REOF
82 climatology, and discuss the properties of the climatologies. We conclude with a summary of
83 our results. Additional details and figures not covered in the main text are included in a
84 Supplementary Material section.

85 86 **2. Ozone data and M2GMI model simulated ozone.**

87 88 **2.1. Aura MLS Ozone.**

89

90 The Microwave Limb Sounder (MLS) instrument onboard the Aura spacecraft makes ozone
91 profile measurements along the orbital track in both daytime and nighttime. Aura is in a sun
92 synchronous orbit, and therefore MLS has nearly complete latitude coverage each day between
93 82°S and 82°N, with local equatorial crossing times of approximately 1:45 pm for the ascending
94 sunlit portion of the orbit and 1:45 am for the nighttime descending node.

95
96 The MLS instrument is a thermal-emission microwave limb sounder that measures vertical
97 profiles of mesospheric, stratospheric, and upper tropospheric temperature, ozone, and several
98 other trace gases from limb scans made ahead of Aura about 7 minutes before the satellite
99 reaches the same point directly below. The MLS instrument primarily uses the 240 GHz
100 microwave band for v4.2 ozone retrievals which for recommended scientific applications extend
101 from 0.0215 hPa to 261 hPa on 38 pressure layers. Vertical spacing for these layers is about 1.3
102 km everywhere below 1 hPa and about 2.7 km at most altitudes above 1 hPa. By comparison,
103 the vertical resolution for the ozone retrievals is reported to be ~3 km extending from 261 hPa up
104 into the mesosphere. Further details regarding the MLS measurements are described by Livesey
105 et al. (2011). The time record for the MLS ozone used in our study was August 2004 –
106 December 2016. Given the high quality of MLS ozone in the low mesosphere we extend the
107 climatology to 80 km from 65 km where the ML climatology ended. We use only MLS
108 measurements at ascending part of the orbit with a local equatorial crossing time at ~1:45 pm.
109 For most latitudes, that corresponds to the daytime measurements ($SZA < 90^\circ$) from MLS in since
110 the daytime data is most appropriate for many passive UV/Vis ozone remote sensing techniques
111 that require daytime measurements. A number of studies of the diurnal ozone variations in
112 stratospheric and mesospheric ozone [Parrish et al., 2014; Frith et al., 2020, and references
113 therein] demonstrated sizeable diurnal ozone variations around 5-10 hPa.

114

115 **2.2. SBUV MOD total ozone record.**

116

117 We use MOD total column ozone measurements from the Solar Backscatter UltraViolet (SBUV)
118 v8.6 retrievals as a proxy to reproduce time-dependent inter-annual variability for the REOF
119 climatology described in Section 4. The MOD total ozone dataset (Frith et al., 2014) is
120 comprised of a composite set of measurements from several SBUV instruments. The first

121 instrument was Nimbus-4 BUV launched in 1970, followed by the second and improved version
122 SBUV on Nimbus-7 launched in October 1978. Starting in 1989, seven SBUV/2 instruments
123 were launched beginning with NOAA-9, followed by NOAA 11, 14, 16, 17, 18, and 19.
124 Currently this record is extended with the Ozone Mapping and Profiler Suite (OMPS) nadir-
125 profiler (NP) on board the Suomi National Polar-orbiting Partnership (SNPP) satellite. There are
126 four follow-up OMPS instrumental suites as a part of JPSS program (with JPSS-1/NOAA-20
127 already in operation) that will extend the SBUV-type ozone observations in the next two
128 decades. The SBUV instruments retrieve broad ozone profiles from measurements of
129 backscattered solar UV radiation which can be integrated to give total column ozone. All MOD
130 instrument measurements have been processed using the v8.6 retrieval algorithm as described by
131 McPeters et al. (2013) and Bhartia et al. (2013). In this study we use monthly zonal-mean
132 gridded total ozone extending from 90°S to 90°N at 5° latitudinal binning (Frith, 2021, personal
133 communication). The MOD total ozone record spans from January 1970 to December 2020 with
134 some temporal gaps, including May 1976-October 1978 due to missing Nimbus-4 BUV
135 measurements.

136

137 **2.3. Ozonesonde measurements.**

138

139 We include balloon-launched ozonesonde measurements for comparison and validation of the
140 M2GMI simulated tropospheric ozone. The used ozonesonde database extends from 2004-2019
141 and includes measurements from the Southern Hemisphere ADditional OZonesondes
142 (SHADOZ) program (Thompson et al., 2017; Witte et al., 2017), the World Ozone and
143 Ultraviolet Data Center (WOUDC) (<https://woudc.org/>), and the Network for the Detection of
144 Atmospheric Composition Change (NDACC). (<http://www.ndsc.ncep.noaa.gov/>). The
145 ozonesondes provide daily ozone profile concentrations generally a few times per week as a
146 function of altitude; we include ozonesonde data from several dozen global sites. Most of the
147 sonde ozone profile measurements that we use are from Electrochemical Concentration Cell
148 (ECC) instruments. The sonde ozone profiles were integrated vertically each day from surface to
149 tropopause to derive tropospheric column ozone (TCO) measurements using the same
150 tropopause pressures as used for M2GMI TCO. Tropopause pressure for both sonde and GMI

151 TCO was derived from National Centers for Environmental Prediction (NCEP) re-analyses based
152 on the World Meteorological Organization (WMO) 2K km⁻¹ temperature lapse-rate definition.

153

154 In section 4 we describe construction of the REOF inter-annual ozone profile climatology that
155 includes monthly tropical Quasi-Biennial Oscillation (QBO) zonal winds. The tropical QBO
156 zonal winds come from the Maldives (January 1970 - December 1975) and Singapore (January
157 1976 - present) rawinsonde record (Univ. Berlin, <https://www.geo.fu-berlin.de/met/>).

158

159 **2.4. MERRA-2 GMI simulated ozone.**

160

161 The M2GMI simulation is produced with the Goddard Earth Observing System (GEOS)
162 modeling framework (*Molod et al., 2015*), using winds, temperature, and pressure from the
163 MERRA-2 reanalysis (*Gelaro et al., 2017*). The configuration for this study is a dynamically
164 constrained replay (*Orbe et al., 2017*) coupled to the Global Modeling Initiative's (GMI)
165 stratospheric and tropospheric chemical mechanism (*Duncan et al., 2007; Oman et al., 2013;*
166 *Nielsen et al., 2017*). The simulation was run at ~0.5° horizontal resolution, on the cubed sphere,
167 and output on the same 0.625° longitude x 0.5° latitude grid as MERRA-2 from 1980-2016. We
168 refer to Strode et al. (2015, 2020) for details of the M2GMI model simulation. The daily
169 M2GMI ozone profiles were averaged monthly and re-gridded from the original resolution to
170 zonal means in 5° latitude bands; the original 72 layers of the simulated profile ozone were also
171 re-mapped to Z* altitudes with 1 km vertical spacing (section 3.2).

172

173 **2.4.1. Evaluation of M2GMI simulated tropospheric ozone.**

174

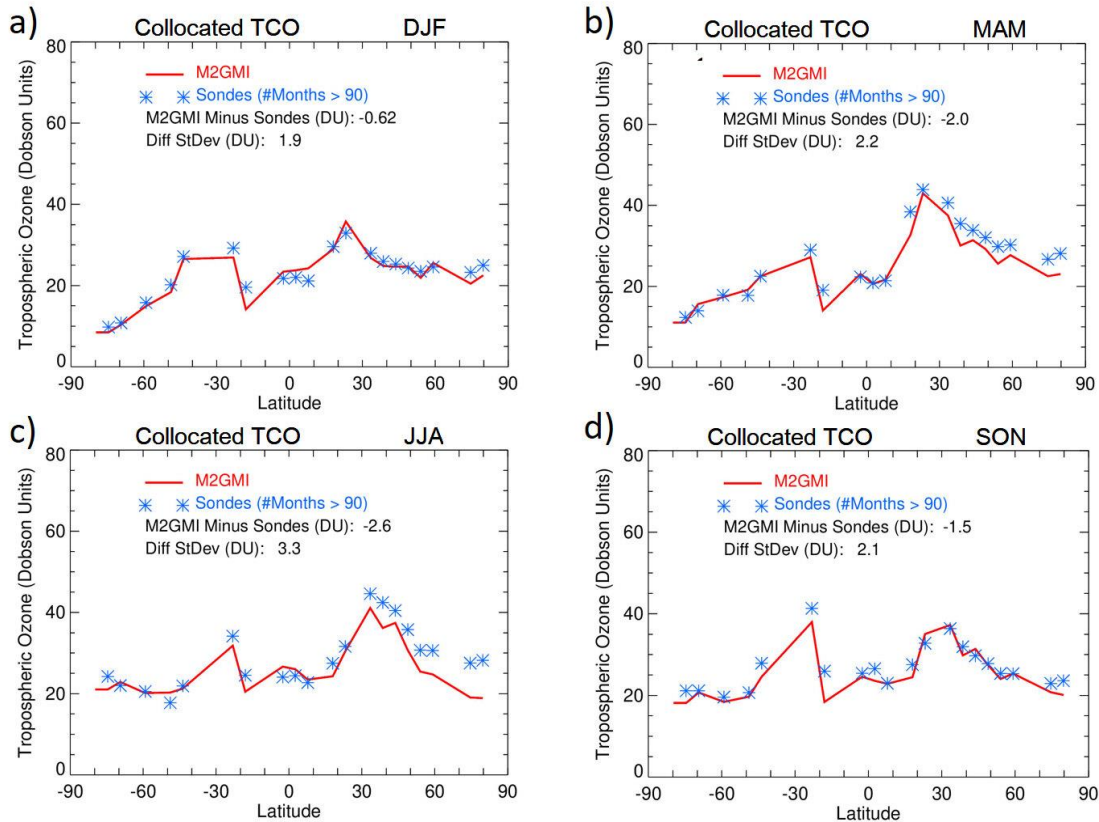
175 Ozone profiles generated by the M2GMI simulation have been extensively evaluated in a
176 number of studies. Stauffer et al. (2019) provide a detailed global analysis of M2GMI ozone
177 profiles using comparisons with ozonesondes. On average they found differences of about ±5%
178 between M2GMI and sondes in the troposphere from 38 sonde stations from 69°S-79°N (their
179 Fig. 1). The largest differences were in the tropics where M2GMI was lower than sonde by up to
180 10-20% in low-mid troposphere, but in the tropical tropopause region M2GMI was higher than
181 sonde by 40-50%; the large percentage differences however can be due to relatively low mean

182 background ozone concentrations of only $\sim 1\text{-}2 \text{ DU km}^{-1}$. Wargan et al. (2018) compared the
183 annual mean ozone mixing ratio anomalies for 1998-2016 between sondes and M2GMI at
184 several stations for 70 hPa, 100 hPa, and 200 hPa. Their comparisons show squared correlations
185 varying from 0.62 to 0.93 and they concluded that the M2GMI simulation well captures the
186 variability of tropospheric ozone including the UTLS region. Ziemke et al. (2014) provide
187 additional evaluation of M2GMI tropospheric ozone by comparing with ozonesondes, satellite,
188 and Global Modeling and Assimilation Office (GMAO) data assimilation; the M2GMI and sonde
189 daily comparisons from tropics to high latitudes in both hemispheres (their Figs. 2-7) showed
190 offsets and standard deviations of differences varying $\sim 0\text{-}2 \text{ DU}$ ($\sim 0\text{-}7\%$) and $4\text{-}7 \text{ DU}$ ($\sim 15\text{-}23\%$),
191 respectively. The M2GMI simulated ozone profiles have also been extensively compared with
192 Atmospheric Tomography Mission (ATom) aircraft flight measurements (Bourgeois et al., 2020)
193 for years 2015 and 2016 (Junhua Liu, personal communication, 2020). The ATom in-flight
194 measurements of ozone volume mixing ratio are found to compare closely with M2GMI
195 simulated ozone, generally within about $\pm 20\%$ along each of the mission flight paths that
196 included meandering ascent and descent between near surface and tropopause each day.

197
198 Our study also includes evaluation of M2GMI simulated tropospheric ozone. Figure 1 compares
199 sonde and M2GMI Tropospheric Column Ozone (TCO) where the sonde and M2GMI
200 measurements have been space-time co-located at the sonde station sites and seasonally averaged
201 for 2004-2016. The collocation involved matching daily TCO from the sondes with M2GMI
202 daily TCO at $5^\circ \times 5^\circ$ gridded resolution interpolated to each sonde latitude-longitude location. As
203 noted in section 2.3, both daily sonde and M2GMI TCO were derived using the same NCEP
204 WMO tropopause pressures.

205
206 The M2GMI modelled ozone in Fig. 1 closely simulates the sonde measured ozone year-round
207 with an exception in the NH mid-high latitudes in MAM and JJA where the simulation tends to
208 underdetermine sonde TCO by $\sim 5 \text{ DU}$ or more. Section S3 of the Supplementary Material
209 includes additional discussion and figures regarding evaluation of M2GMI tropospheric ozone
210 profiles using ozonesondes and surface lidar measurements.

211



212

213 **Figure 1.** Comparisons between M2GMI simulated (red curves) and ozonesonde TCO (blue
 214 asterisks) averaged over three-month seasons (indicated) for 2004-2016. The M2GMI TCO field
 215 is sampled daily at the sonde station locations. All TCO is in Dobson Units. The same daily
 216 tropopause is used for both M2GMI and sonde to derive TCO, and is defined as according to the
 217 WMO 2 K km⁻¹ lapse-rate tropopause definition using NCEP temperatures. Included in each
 218 panel are mean offsets and standard deviations of TCO seasonal differences.

219

220 **3. The MLS/GMI seasonal climatology.**

221

222 The MLS/GMI seasonal climatology product is derived for both volume mixing ratio (units
 223 ppmv) and vertical column concentration (DU km⁻¹); the latter has vertical and latitudinal
 224 structure that is closely similar to that of ozone number density and ozone partial pressure.
 225 Standard deviations are reported for both mixing ratios and column concentrations based upon
 226 all available daily ozone profiles over a given month and within every 5° latitude band. The
 227 standard deviations provide a measure of climatological ozone variability and are important for

228 error covariance matrices included as a priori information in retrieval algorithms such as the
229 optimal estimation method of Rodgers (2000). We refer the reader to the Supplementary
230 Materials for further discussion and figures involving calculated standard deviations.

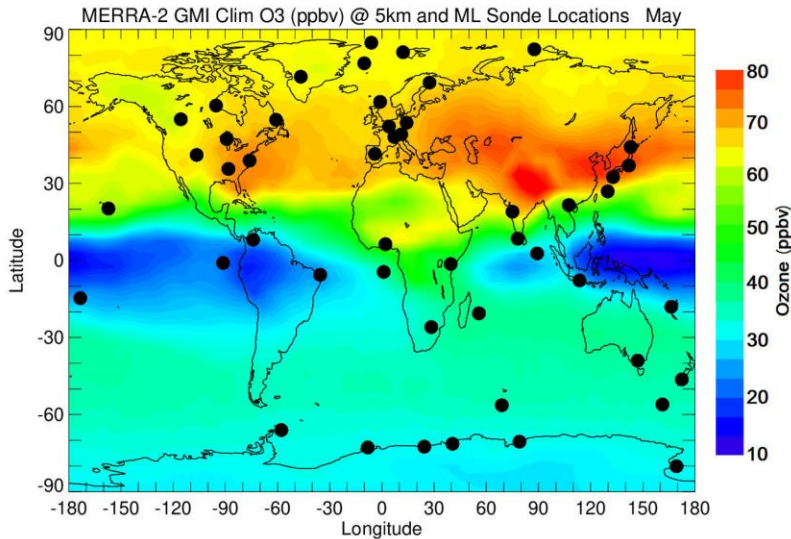
231

232 3.1. Global coverage of M2GMI tropospheric ozone compared to sondes.

233

234 Our motivation for using M2GMI simulation is that they provide better spatial and temporal
235 representation of tropospheric ozone profiles than ozonesondes. The sondes are sparsely
236 distributed over the Earth with generally only a few measured profiles per month for a given
237 station. The limited spatial coverage of sondes is demonstrated in Fig. 2 with M2GMI mid-
238 tropospheric ozone concentration (ppbv) at height $Z^*=5$ km for climatological May (Z^* is
239 approximately equal to actual altitude and is defined in section 3.2.)

240



241

242 **Figure 2.** Map of climatological ozone volume mixing ratio (in ppbv) from the M2GMI
243 simulation at $Z^*=5$ km altitude (see section 3.2) for the month of May. Blue color indicates areas
244 with ozone concentration of about 10 ppbv and red color corresponds to regions with > 75 ppbv.
245 Black circles show locations of the sonde stations with a long observational record. Data from
246 these stations were used to constrain tropospheric ozone profiles in the ML climatology.

247

248 Tropospheric ozone exhibits planetary-scale variability that includes a year-round zonal wave-1
249 pattern in the tropics (greatest amplitude in September-October) and large-scale patterns outside
250 the tropics that vary greatly with season and region (Fishman et al., 1990). The tropical wave-1
251 in tropospheric ozone originates from regional sources of ozone: lightning, biofuel & biomass
252 burning, stratosphere-troposphere exchange (STE), and transport associated with the tropical
253 east-west Walker circulation. In the extra-tropics, the large planetary scale features in
254 tropospheric ozone have strong seasonal dependence with the seasonal maximum in JJA in the
255 NH and SON in the SH. These seasonal patterns in tropospheric ozone outside the tropics are
256 also due to combined effects from STE, biofuel, lightning, biomass burning, and long-range
257 transport. The global planetary-scale patterns in tropospheric ozone columns were first shown
258 from TOMS/SAGE (Fishman et al., 1990) and TOMS/MLS (Ziemke et al., 1996) satellite
259 measurements. The patterns in the M2GMI tropospheric ozone mixing ratio for $Z^* = 5$ km in
260 Fig. 2 in the tropics and in the NH are similar to the TCO May pattern from satellite records.

261
262 It is apparent from Fig. 2 that the ensemble of ozonesondes is unlikely to effectively represent
263 the zonal mean tropospheric ozone values due to their limited sampling. For example, in the
264 tropics the sonde measurements under-sample the tropical wave-1 structure in tropospheric
265 ozone. Due to the under-sampling in the tropical Pacific area, sondes do not capture the very
266 low ozone concentrations of ~ 10 ppbv. This leads to the over-estimation of zonal-mean
267 tropospheric ozone in the tropics from the sondes. We will show later that this over-
268 determination of ML tropospheric ozone in the tropics averages to about 5-10 DU in TCO year-
269 round between 20°S - 20°N . The sondes also tend to miss the high values of ozone in the NH
270 mid-latitudes over the Asian continent (see Fig. 2), thus introducing a low bias in zonal-mean
271 tropospheric ozone in NH mid-latitudes.

272

273 **3.2. Merging MLS and M2GMI ozone profiles.**

274

275 Simulated ozone volume mixing ratio values from the M2GMI model were merged with ozone
276 volume mixing ratio measurements from MLS to construct the ozone profile seasonal
277 climatology in the format of monthly zonal means. The merging of MLS and M2GMI ozone
278 involved monthly zonal-mean ozone profiles for both records in 5° latitude bands with Z^*

279 altitudes 0-80 km (1 km increments). For low and mid-latitudes between 40°N and 40°S the
280 M2GMI and MLS profiles were merged for Z^* levels between 13 km and 21 km (156 hPa to
281 49 hPa). For latitudes poleward of 40° in each hemisphere the profiles were merged slightly
282 lower in the atmosphere, for Z^* levels between 8 km and 16 km (320 hPa to 101 hPa). Within
283 the merged altitude ranges the climatology is weighted linearly, from 100% M2GMI at the
284 lowest altitude to 100% MLS at the highest altitude. Standard deviations were calculated for
285 each climatological ozone value.

286
287 As in previous climatologies, the altitude variable used for our climatology is Z^* , a parameter
288 frequently used in comparisons of atmospheric chemistry models (Park et al., 1999). Z^* is in
289 units of kilometers but can be considered a pressure variable. $Z^*(\text{km})$ is defined by
290 $Z^* = 16 \cdot \log(1013/P)$ where P is atmospheric pressure in units hPa. The altitude spacing for our
291 climatology is 1 km in Z^* units. In an isothermal terrestrial atmosphere Z^* would correspond
292 closely to altitude.

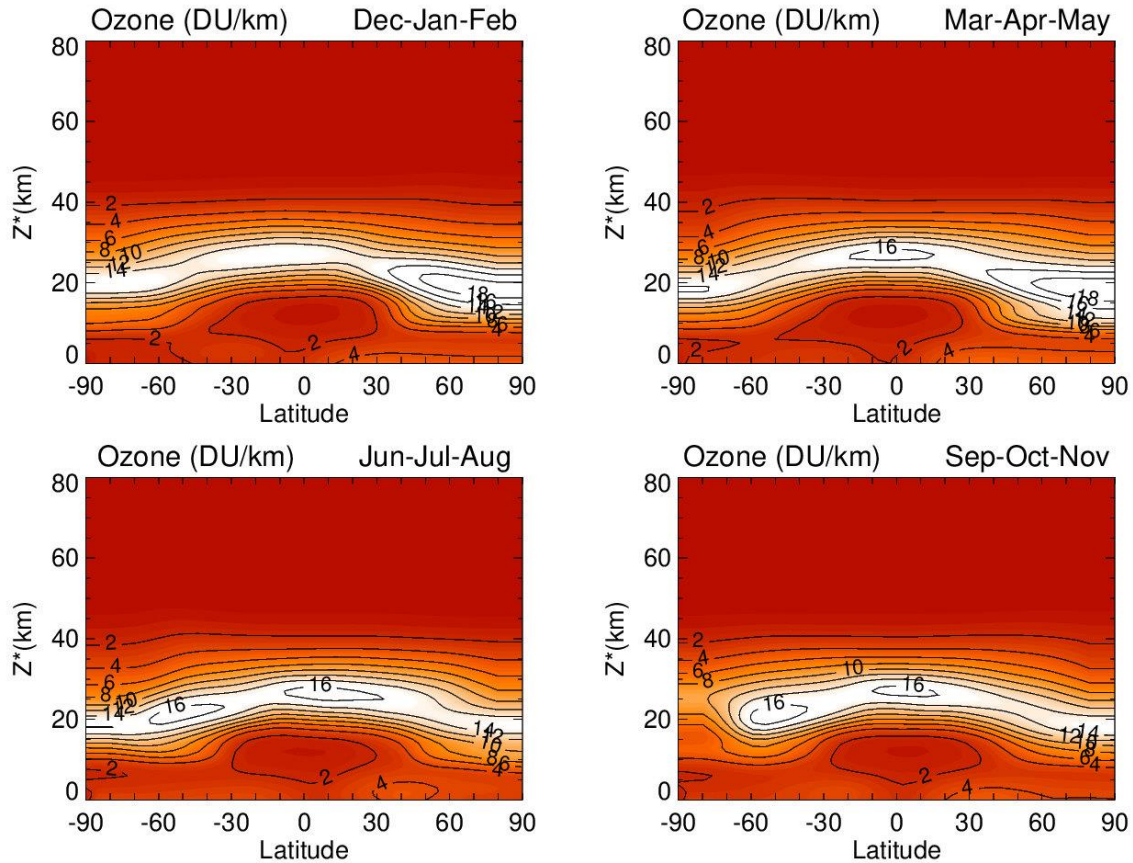
293

294 **3.3. Comparisons with the ML Climatology.**

295

296 We first examine basic global patterns of the MLS/GMI seasonal climatology. Figure 3 shows
297 vertical column concentrations (DU km^{-1}) for the climatology by 3-month season (indicated) for
298 $Z^* = 0\text{-}80$ km. Column concentrations in the low stratosphere in both hemispheres are largest
299 during winter-spring and smallest in summer. In both hemispheres, ozone is largest in the
300 winter-spring months due to seasonal transport from the tropics to the extra-tropics in winter-
301 spring months (i.e., the Brewer Dobson Circulation) and longer lifetimes for ozone in the low
302 stratosphere. The highest ozone amounts in Fig. 3 are $\sim 18\text{-}20 \text{ DU km}^{-1}$ in the NH around 20 km
303 during winter and spring. In the troposphere, very low ozone density of less than 2 DU km^{-1}
304 occurs in the tropics year-round.

305



306

307 **Figure 3.** Meridional cross-sections of derived zonal-mean vertical ozone concentration (units
 308 DU km^{-1}) for the MLS/GMI seasonal climatology. This 12-month climatology is averaged over
 309 three-month seasons (indicated) for 2004-2016 and is binned for 5° latitude bands and Z^* levels
 310 from 0-80 km at 1 km spacing (see text).

311

312 While the basic characteristics of stratospheric ozone in Fig. 3 are important to note, our main
 313 focus is to compare tropospheric ozone in Fig. 3 with the ML sonde ozone climatology. Because
 314 the ML climatology uses sparsely sampled sonde measurements to estimate zonal-means in the
 315 troposphere, it is possible that there may be substantial differences.

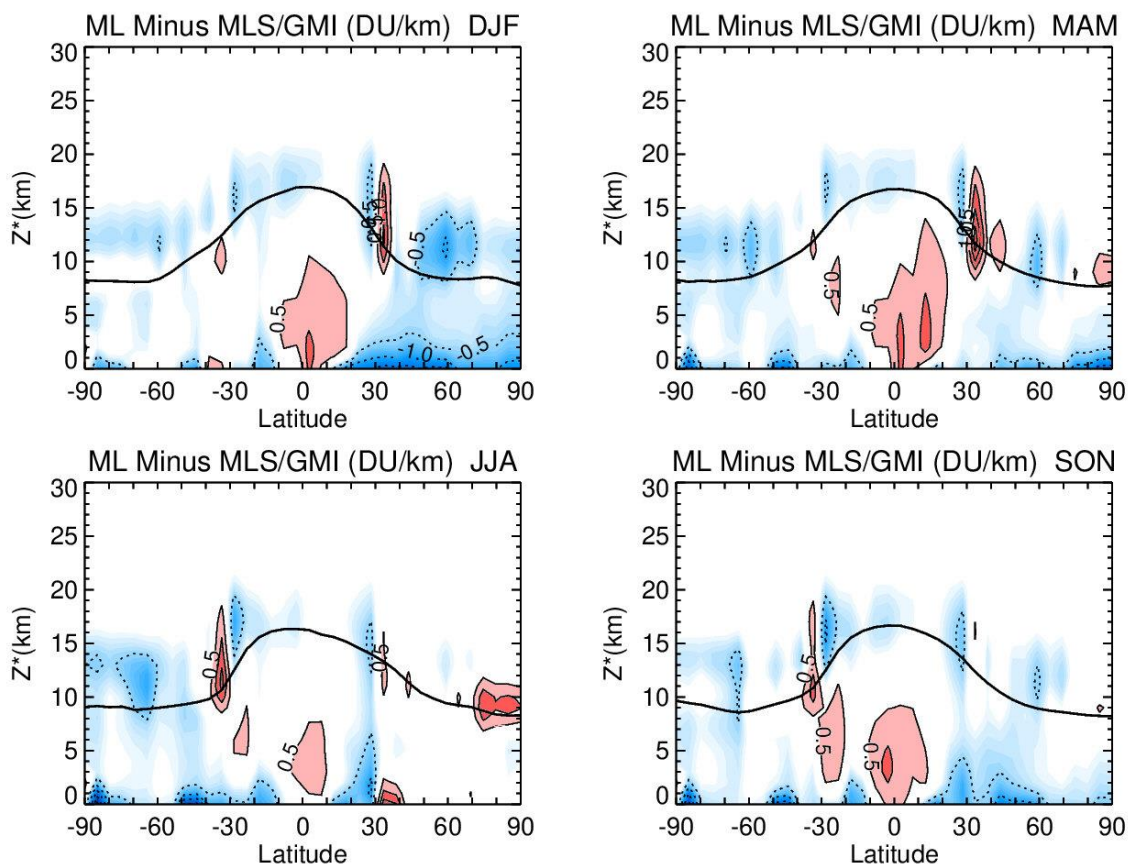
316

317 Figure 4 shows the difference between ML and MLS/GMI zonal-mean profile ozone by season,
 318 plotted as Z^* altitude versus latitude. Only Z^* levels 0-30 km are included in Fig. 4 to highlight
 319 differences in ozone profiles used for the troposphere and the low stratosphere merging region.

320 Year-round positive differences in the tropics in Fig. 4 suggest that ML is always too large in the

321 low-mid troposphere compared to M2GMI due to absence of ML sonde measurements in the
 322 Pacific region where tropospheric ozone is low (e.g., Fig. 2). At latitudes around $\pm 35^\circ$ and
 323 elsewhere in the low stratosphere merging region in Fig. 4 there are anomalous differences from
 324 -0.5 up to $+1.5$ DU km^{-1} ; these sharp patterns are ascribed to sonde sampling issues for the ML
 325 climatology. In the boundary layer throughout the NH extra-tropics during winter (i.e., upper
 326 left panel in Fig. 4) the M2GMI ozone is higher than sondes by ~ 0.5 to 1 DU km^{-1} . These latter
 327 differences are attributed to a known model issue related to underestimating surface deposition
 328 over cold surfaces (Jaegle et al. 2018), most prominent in the NH boundary layer during winter.
 329 When compared with ML in Fig. 4, the model in this region over-determines the ozone column
 330 in DJF by about 2 DU.

331

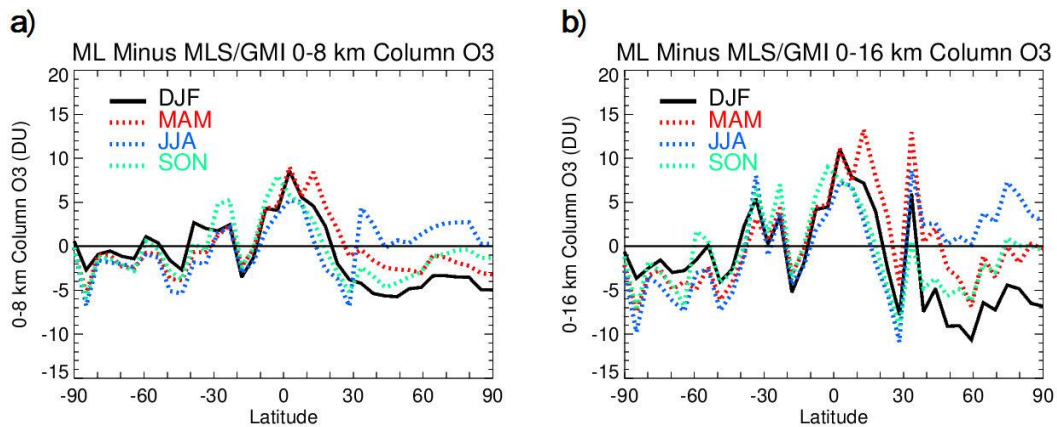


332
 333 **Figure 4.** Meridional cross-sections of ML minus MLS/GMI climatologies of ozone column
 334 concentration (DU km^{-1}). These differences are averaged over three-month seasons (indicated)
 335 for 2004-2016 and are binned for 10° latitude bands and Z^* levels from 0-30 km at 1 km spacing.

336 Contour levels (indicated) increment by 0.5 DU km^{-1} with blue/dashed contours meaning
337 negative, and pink/red solid contours meaning greater than 0.5 DU km^{-1} . The black line indicates
338 tropopause height according to the WMO 2 K km^{-1} lapse-rate tropopause definition using NCEP
339 temperatures. White color denotes zero differences.

340
341 Line plots of seasonal differences (ML minus MLS/GMI) of integrated ozone columns are
342 shown in Fig. 5 for 0-8 km (Fig. 5a) and 0-16 km (Fig. 5b). These line plots are determined from
343 Fig. 4 by summing the 1 km layers of ML minus MLS/GMI differences. In the tropics 0-16 km
344 integrated column in Fig. 5b represents the total troposphere (i.e., TCO) with ML larger than
345 MLS/GMI by about 10 DU year-round. Comparison with the 0-8 km columns in the left panel
346 show that these differences in the tropics originate mostly from the lower troposphere which is
347 consistent with all four panels in Fig. 4. Outside the tropics in Fig. 5 there are seasonal offset
348 differences in the NH up to -5 to -10 DU during DJF. Part of the reason for the ML minus
349 MLS/GMI biases in Fig. 5 is due to sonde under-sampling for the ML climatology, particularly
350 in the tropics as noted for Fig. 4. The sonde under-sampling also creates the sharp (non-physical)
351 variability seen between adjacent latitude bins in Fig. 5.

352



353

354 **Figure 5.** (a) Line plots of seasonal differences of ML minus MLS/GMI integrated ozone
355 columns for 0-8 km. The differences are averaged over three-month seasons (indicated by DJF,
356 MAM, JJA, and SON). (b) Same as (a), but for 0-16 km ozone columns.

357

358 **4. An inter-annual ozone profile climatology.**

359

360 The MLS/GMI seasonal climatology captures the vertical shape of zonal-mean ozone profiles by
361 season and latitude in both troposphere and stratosphere. However, inter-annual processes such
362 as the QBO produce sizeable changes in the vertical ozone distribution in stratospheric ozone
363 from year to year. To capture these variations, we have constructed a global time-dependent
364 climatology of stratospheric ozone that represents ozone inter-annual variability. This
365 climatology can be used either independently or added to the MLS/GMI seasonal climatology,
366 depending on the particular application.

367
368 The derivation of the inter-annual ozone climatology is lengthy and is discussed in detail in the
369 Supplementary Materials. In this section we provide only a short overview of the methodology
370 and discuss the final product. The inter-annual ozone climatology is constructed using a method
371 that includes an REOF analysis as described by Richman (1986, and references therein). With
372 our approach, vertical information for the climatology comes from an REOF analysis of MLS
373 ozone profiles, while month-to-month time dependence follows by coupling the REOF analysis
374 time coefficients with SBUV MOD total ozone and tropical QBO zonal winds. The time period
375 for the REOF climatology depends on the availability of total ozone and tropical QBO winds.
376 The time period for this climatology is 1970-2018 (588 consecutive months) with gaps present
377 due to some missing MOD total ozone including Nimbus 4 measurements in the 1970s. We plan
378 to periodically extend this REOF climatology when zonal wind and MOD total ozone data
379 become available. Before applying the REOF approach, an Empirical Orthogonal Function
380 (EOF) method (Kutzbach 1967, and references therein) was applied to MLS ozone anomaly
381 profiles to derive repeatable inter-annual patterns in the ozone vertical distribution; that is, the
382 EOF analysis was applied to MLS monthly zonal-mean ozone profile anomalies derived by
383 removing seasonal cycles between August 2004 and December 2016. All MLS ozone and
384 anomaly ozone profiles were binned into 5° latitude bands (36 bands for 90°S-90°N, similar to
385 MLS/GMI climatology) between 1 and 261 hPa (30 pressure levels).

386
387 The main challenge of EOF analysis is interpretation of derived EOFs and EOF time coefficients
388 and their attribution to specific geophysical processes. As described in the Supplementary
389 Materials, the construction of this REOF climatology required only total ozone and tropical
390 stratospheric zonal wind time series to explain most of stratospheric ozone profiles variability

391 (total EOF variance). We used MLS ozone anomalies expressed as ozone partial pressure for the
392 REOF analysis rather than ozone mixing ratio because it helped to attribute the REOF-1 time
393 coefficient directly to total ozone column measurements at all latitudes. The first REOF vector
394 with the MOD total ozone time series as a proxy explains about 50-70% of the inter-annual
395 ozone variability. -Next, we derived a second REOF-2 that we attributed to the QBO and used
396 the equatorial zonal wind time series as a proxy for REOF-2. The sum of these two REOFs
397 explains about 70-80% of the inter-annual variability in de-seasonalized MLS zonal mean ozone
398 profiles. Since only MLS profiles are used to constrain the vertical shapes of the REOFs and
399 time coefficients are described by total ozone and zonal winds, this REOF climatology can be
400 used in the future (even after MLS stops operating) or can be extended into the past to the pre-
401 Aura time period whenever total column ozone and wind data are available.

402
403 The REOF climatology was finally converted from the ozone partial pressures defined at 30
404 MLS levels to volume mixing ratio (ppmv) and partial ozone column (DU km^{-1}) at the $1 \text{ km } Z^*$
405 levels (defined in section 3.2) identical to the MLS/GMI climatology. The REOF climatological
406 values at levels below $\sim 9 \text{ km}$ and above $\sim 48 \text{ km}$ are very small in contributing to inter-annual
407 variability of ozone and are set to zero. Since the REOF climatology uses zonal wind and total
408 ozone time series that can have long-term trends, we applied a very low frequency (VLF) digital
409 low-pass filter to the final derived REOF climatology to remove long-term decadal variability.
410 This was done to ensure that the climatology captures only inter-annual variability in monthly
411 zonal mean ozone anomaly profiles without inducing decadal trends if used as a prior in ozone
412 retrieval. The frequency response of the applied VLF digital filter (Stanford and Ziemke, 1993)
413 is exactly 0.0 (1.0) at zero (Nyquist) frequency with an amplitude of 0.5 at frequency 0.00333
414 month^{-1} ; the filter was also designed to have zero phase shift at all frequencies.

415
416 We demonstrate that the REOF climatology does very well in capturing inter-annual variability
417 of monthly zonal-mean stratospheric ozone. The high vertical resolution of MLS ozone limb
418 measurements of $\sim 3 \text{ km}$ resolves much of the vertical variability of ozone caused by low-
419 frequency and episodic processes such as the QBO, extra-tropical stratospheric warmings, and
420 other year-round planetary-scale wave events (e.g., Ziemke et al., 2014, and references therein).
421 Many nadir instrument ozone profile retrievals have coarse vertical resolution of ~ 6 to 10 km or

422 greater (such as from SBUV or OMI) and cannot do nearly as well at resolving vertical changes
423 in stratospheric ozone.

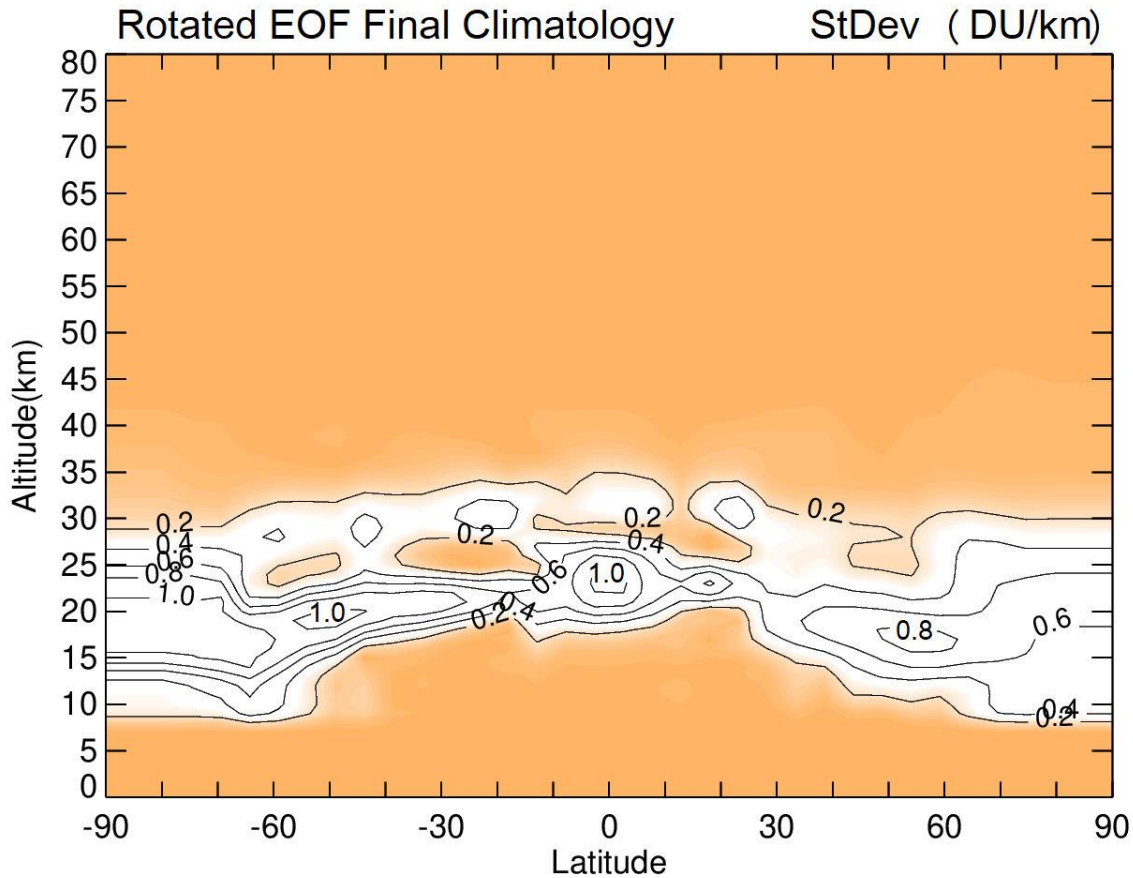
424

425 The magnitude of inter-annual variability in profile ozone, captured by the REOF climatology, is
426 shown in Fig. 6 as calculated standard deviations in DU km⁻¹ for the 1970-2018 period. In the
427 tropical low latitudes from 10°S-10°N the main source of inter-annual variability is the QBO.
428 However, larger inter-annual variability occurs in the SH extra-tropics due to the QBO and
429 additional dynamical sources. In an effort to understand the contribution of non-QBO processes
430 to the inter-annual variability we also generated a climatology using only equatorial QBO zonal
431 winds as a proxy (see Fig. S4 in the Supplementary Material). When compared to the REOF
432 climatology in Fig. 6, only a very small fraction of inter-annual variability is captured in the
433 extra-tropics for the QBO-only climatology.

434

435

436

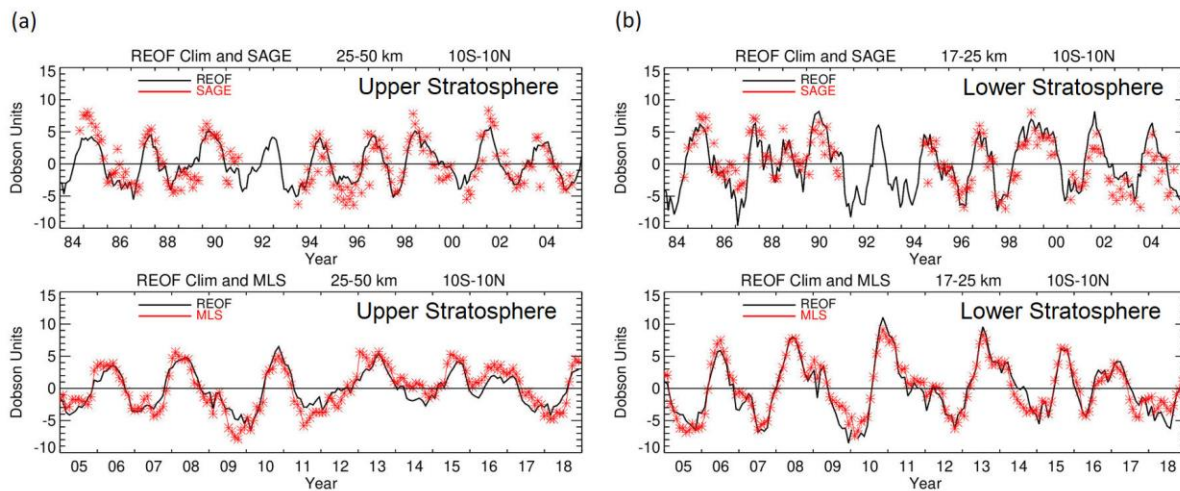


437
 438 **Figure 6.** Temporal standard deviation (in DU km⁻¹) for 1970-2018 for the final REOF ozone
 439 climatology (i.e., Eq. (S10) in Supplementary Materials). The inter-annual variability in the
 440 tropical low latitudes is almost entirely due to the QBO. Inter-annual variability in the extra-
 441 tropics comes from the QBO coupled with other non-QBO related inter-annual variability.

442
 443 The long record of the REOF inter-annual ozone profile climatology has been compared with de-
 444 seasonalized ozone profile measurements from SAGE II and Aura MLS for 1984-2018 (Fig. 7).
 445 The top panel in Fig. 7a shows comparisons of upper stratospheric column ozone anomalies
 446 ($Z^* = 25-50$ km) between REOF (black curve) and SAGE (red asterisks) for years 1984-2005 in
 447 the tropics (10°S-10°N). The bottom panel in Fig. 7a shows a similar comparison between
 448 REOF and MLS for 2005-2018. Figure 7b is the same as in Fig. 7a, except for the lower
 449 stratosphere ($Z^* = 17-25$ km).

450

451 The SAGE II sampling ozone columns in Fig. 7 is sparse, averaging ~2-3 days of measurements
 452 for a given month in the 10°S-10°N latitude band shown. This means that the monthly SAGE
 453 measurements in Fig. 7 are more representative of daily profiles rather than monthly means.
 454 Ozone profiles on a daily basis in the tropics are distorted by propagating tropical waves with
 455 periods of days to weeks such as Kelvin waves, equatorial Rossby waves, and mixed Rossby-
 456 gravity waves (e.g., Timmermans et al., 2005; Ziemke and Stanford, 1994). As a result, the
 457 upper and lower stratospheric columns in Fig. 7 for SAGE II will have noisy month-to-month
 458 variations of several DU because of these tropical waves. The Supplementary Material includes
 459 further discussion and figures for the REOF climatology.
 460



461
 462 **Figure 7.** (a) Top panel is zonal-mean upper stratospheric column ozone (in Dobson Units) for
 463 the REOF climatology (black curve) and deseasonalized SAGE II (red asterisks) spanning 1984-
 464 2005 and averaged between 10°S-10°N. The SAGE data are deseasonalized monthly zonal
 465 means. All column amounts are calculated by integrating ozone profiles for $Z^*=25-50$ km (~28
 466 to 1 hPa). Bottom panel is the same as the top panel, but with MLS in place of SAGE and for the
 467 time period 2005-2018. (b) Same as (a), but for the lower stratosphere with $Z^*=17-25$ km (~88
 468 to 28 hPa).

469
 470 **5. Summary.**

471

472 We have produced a new MLS/GMI seasonal ozone profile climatology by combining ozone
473 profiles from the M2GMI model simulation with MLS v4.2 measurements. M2GMI is used
474 primarily for tropospheric ozone and MLS for stratospheric ozone, with the two ozone profile
475 datasets blended together in the low stratosphere; the result is a merged zonal-mean, 12-month
476 global ozone profile climatology at 5° latitude resolution with Z* altitude range 0-80 km (1 km
477 vertical sampling). Our main interest in generating the MLS/GMI climatology is to use it as a
478 priori information in satellite ozone retrieval algorithms. However, it is also useful as a baseline
479 for evaluating various modeled or measured ozone seasonal and inter-annual variability, and in
480 studies involving corresponding ozone radiative forcing as inferred from atmospheric radiative
481 transfer calculations.

482
483 In previous studies we generated several ozone profile climatologies based on combining
484 ozonesondes with either SAGE or MLS satellite measurements (e.g., McPeters et al., 2007;
485 McPeters and Labow, 2012; Labow et al., 2015). We have compared the new MLS/GMI
486 climatology in detail with the ML climatology of McPeters and Labow (2012) that used
487 ozonesondes for tropospheric ozone profiles. The M2GMI model simulation provides an
488 improved ozone climatology for the troposphere compared to the ML climatology due to having
489 much better spatial and temporal coverage than the sondes.

490
491 We also developed a time-dependent climatology of monthly zonal-mean profile ozone
492 anomalies representing inter-annual variability. This inter-annual climatology was constructed
493 using a rotational EOF analysis of Aura MLS monthly zonal-mean profile ozone anomalies from
494 August 2004 – December 2016 within each 5° latitude band. The analysis shows that the first
495 two leading EOFs explain ~70-80% of inter-annual variability of profile ozone at all latitudes.
496 Furthermore, total ozone and tropical zonal wind time series correlate well with the two leading
497 EOF coefficient time series and were used as proxies to extend information outside the Aura
498 MLS time range. We used these relationships to reconstruct anomalies at 5° latitudinal resolution
499 for Z* = 0-80 km and 1970-2018. This REOF time-dependent climatology was compared to a
500 similar climatology based on only tropical QBO winds. The advantage of the REOF climatology
501 is that allows for a much more thorough representation of inter-annual variability of stratospheric
502 ozone than just the QBO.

503
504
505
506
507
508
509
510
511
512
513
514
515
516
517
518
519
520
521
522
523
524
525
526
527
528
529
530
531
532

The REOF time-dependent climatology of ozone profile anomalies can be easily added to the MLS/GMI seasonal climatology to simulate seasonal+inter-annual variability of stratospheric ozone. We note that both the MLS/GMI 12-month climatology and REOF climatology were generated using Aura time period MLS ozone measurements and neither of them account for long-term trends in stratospheric ozone.

Code availability. Codes used to generate the ozone climatologies along with the analyses in this study are available upon personal request to J. Ziemke (gerald.r.ziemke@nasa.gov).

Data availability. Data description for MLS v4.2 ozone and links to the data can be obtained from websites https://mls.jpl.nasa.gov/products/o3_product.php (last access 16 April 2021) and <https://disc.gsfc.nasa.gov/> (last access 16 April 2021). MERRA-2 GMI model description and access is available at <https://acd-ext.gsfc.nasa.gov/Projects/GEOSCCM/MERRA2GMI/> (last access: 16 April 2021). The MOD total ozone measurements are available from the webpage https://acd-ext.gsfc.nasa.gov/Data_services/merged/. Tropical QBO winds were provided by the University of Berlin from <https://www.geo.fu-berlin.de/met/ag/strat/produkte/qbo/qbo.dat>. The seasonal and inter-annual climatology products derived from our study are available for the general public using direct links from the NASA webpage <https://avdc.gsfc.nasa.gov/>.

Executable research compendium (ERC). N/A

Sample availability. N/A

Video supplement. N/A

Supplement link. N/A

Team list. N/A (no team associated with this work)

533 **Author contribution.** J. Ziemke is the leading author of the paper and was responsible for
534 writing the paper and data analysis for the paper that included development of the REOF inter-
535 annual climatology and validation. G. Labow was responsible for help in writing the paper and
536 development of the MLS/GMI seasonal climatology and providing the ozonesonde database used
537 for validation. N. Kramarova was also responsible for writing the paper and analyses of total
538 ozone and tropospheric ozone, and the derived climatologies. R. McPeters and P. K. Bhartia as
539 experts in ozone algorithms contributed to the analysis that included their extensive experiences
540 in developing ozone climatologies and applications involving the rotational EOF technique. L.
541 Oman also helped with the analysis and the writing of the paper regarding especially the M2GMI
542 simulated ozone. S. Frith and D. Haffner had key roles involving analysis of the derived
543 seasonal and REOF climatologies.

544

545 **Competing interests.** No competing interests.

546

547 **Disclaimer.** N/A

548

549 **Special issue statement.** N/A

550

551 **Acknowledgments.** We thank the NASA Jet Propulsion Laboratory MLS team for the MLS
552 v4.2 ozone dataset and the SHADOZ, WOUDC and NDACC personnel for providing the
553 extensive ozonesonde measurements that we used for our study. We also thank the NASA MAP
554 program for supporting the MERRA-2 GMI simulation and the NASA Center for Climate
555 Simulation (NCCS) for providing high-performance computing resources. Special thanks go to
556 the NASA GMI group especially Sarah Strode regarding the MERRA-2 GMI simulation.
557 Funding for this research was provided in part by NASA NNH14ZDA001N-DSCOV.

558

559 **References.**

560

561 Bass, A. M., and R. J. Paur, The ultraviolet cross-sections of ozone, I: The measurements, in
562 *Proc. Quad. Ozone Symp.*, edited by C. Zerefos, and A. Ghazi, pp. 606–616, Reidel, Dordrecht,
563 Halkidiki, Greece, 1984.

564
565 Bourgeois, I., J. Peischl, C. R. Thompson, K. C. Aikin, T. Campos, H. Clark, R. Commane, B.
566 Daube, G. W. Diskin, J. W. Elkins, R.-S. Gao, A. Gaudel, E. J. Hintsä, B. J. Johnson, R. Kivi, K.
567 McKain, F. L. Moore, D. D. Parrish, R. Querel, E. Ray, R. Sánchez, C. Sweeney, D. W.
568 Tarasick, A. M. Thompson, V. Thouret, J. C. Witte, S. C. Wofsy, and T. B. Ryerson, Global-scale
569 distribution of ozone in the remote troposphere from the ATom and HIPPO airborne field
570 missions *Atmos. Chem. Phys.*, 20, 10611–10635, <https://doi.org/10.5194/acp-20-10611-2020>,
571 2020.
572
573 Duncan, B. N., R. V. Martin, A. C. Staudt, R. Yevich, and J. A. Logan, Interannual and seasonal
574 variability of biomass burning emissions constrained by satellite observations, *J. Geophys. Res.*
575 *Atmos.*, 108(D2), doi:10.1029/2002jd002378, 2003.
576
577 Duncan, B.N., S.E. Strahan, Y. Yoshida, S.D. Steenrod, and N. Livesey, Model study of cross-
578 tropopause transport of biomass burning pollution, *Atmos. Chem. Phys.*, 7, 3713-3736,
579 doi:10.5194/acp-7-3713-2007, 2007.
580
581 Fishman, J., C. E. Watson, J. C. Larsen, and J. A. Logan, Distribution of tropospheric ozone
582 determined from satellite data, *J. Geophys. Res.*, 95(D4), 3599-3617, 1990.
583
584 Frith, S. M., N. A. Kramarova, R. S. Stolarski, R. D. McPeters, P. K. Bhartia, and G. J. Labow,
585 Recent changes in total column ozone based on the SBUV Version 8.6 Merged Ozone Data Set,
586 *J. Geophys. Res. Atmos.*, 119, 9735–9751, doi:10.1002/2014JD021889, 2014.
587
588 Frith, S. M., P. K. Bhartia, L. D. Oman, N. A. Kramarova, R. D. McPeters, and G. J. Labow,
589 Model-based climatology of diurnal variability in stratospheric ozone as a data analysis tool
590 *Atmos. Meas. Tech.*, 13, 2733–2749, <https://doi.org/10.5194/amt-13-2733-2020>, 2020.
591
592 Froidevaux, L., et al., Validation of Aura Microwave Limb Sounder stratospheric ozone
593 measurements, *J. Geophys. Res.*, 113, D15S20, doi:10.1029/2007JD008771, 2008.
594

595 Gelaro, R., W. McCarty, M.J. Suárez, R. Todling, A. Molod, L. Takacs, C.A. Randles, A.
596 Darmenov, M.G. Bosilovich, R. Reichle, K. Wargan, L. Coy, R. Cullather, C. Draper, S. Akella,
597 V. Buchard, A. Conaty, A.M. da Silva, W. Gu, G. Kim, R. Koster, R. Lucchesi, D. Merkova, J.E.
598 Nielsen, G. Partyka, S. Pawson, W. Putman, M. Rienecker, S.D. Schubert, M. Sienkiewicz, and
599 B. Zhao, The Modern-Era Retrospective Analysis for Research and Applications, Version 2
600 (MERRA-2), *J. Climate*, 30, 5419–5454, <https://doi.org/10.1175/JCLI-D-16-0758.1>, 2017.
601

602 Giglio, L., J. Randerson, and G. van der Werf, Analysis of daily, monthly, and annual burned
603 area using the fourth-generation global fire emissions database (GFED4), *J. Geophys. Res.*
604 *Bio.Sci.*, 118(1), 317-328, doi:10.1002/jgrg.20042, 2013.
605

606 Granier, C., B. Bessagnet, T. Bond, A. D’Angiola, H. D. van der Gon, et al., Evolution of
607 anthropogenic and biomass burning emissions of air pollutants at global and regional scales
608 during the 1980–2010 period. *Climatic Change*, 109, 163–190, doi:10.1007/s10584-011-0154-1,
609 2011.
610

611 Jaeglé, L., V. Shah, J. A. Thornton, F. D. Lopez-Hilfiker, B. H. Lee, E. E. McDuffie, et al.,
612 Nitrogen oxides emissions, chemistry, deposition, and export over the Northeast United States
613 during the WINTER aircraft campaign, *J. Geophys. Res. Atmos.*, 123, 12,368–12,393,
614 <https://doi.org/10.1029/2018JD029133/>, 2018.
615

616 Jiang, Y. B., et al., Validation of Aura Microwave Limb Sounder Ozone by ozonesonde and lidar
617 measurements, *J. Geophys. Res.*, 112, D24S34, doi:10.1029/2007JD008776, 2007.
618

619 Kutzbach, J. E., Empirical eigenvectors of sea-level pressure, surface temperature and
620 precipitation complexes over North America, *J. App. Meteorol.*, 6, 791-802,
621 [https://doi.org/10.1175/1520-0450\(1967\)006<0791:EEOSLP>2.0.CO;2](https://doi.org/10.1175/1520-0450(1967)006<0791:EEOSLP>2.0.CO;2), 1967.
622

623 Labow, G. J., J. R. Ziemke, R. D. McPeters, D. P. Haffner, and P. K. Bhartia, A total ozone-
624 dependent ozone profile climatology based on ozonesondes and Aura MLS data, *J. Geophys.*
625 *Res. Atmos.*, *120*, 2537-2545, doi:10.1002/2014JD022634, 2015.

626

627 Lamarque, J.-F., T. C. Bond, V. Eyring, C. Granier, A. Heil, Z. Klimont, D. Lee, C. Liousse, A.
628 Mieville, B. Owen, M. G. Schultz, D. Shindell, S. J. Smith, E. Stehfest, J. Van Aardenne, O. R.
629 Cooper, M. Kainuma, N. Mahowald, J. R. McConnell, V. Naik, K. Riahi, and D. P. van Vuuren,
630 Historical (1850-2000) gridded anthropogenic and biomass burning emissions of reactive gases
631 and aerosols: methodology and application, *Atmos. Chem. Phys.*, *10*(15), 7017-7039,
632 doi:10.5194/acp-10-7017-2010, 2010.

633

634 Livesey, N. J., Read, W. G., Froidevaux, L., Lambert, A., Manney, G. L., Pumphrey, H. C.,
635 Santee, M. L., Schwartz, M. J., Wang, S., Cofield, R. E., Cuddy, D. T., Fuller, R. A., Jarnot, R.
636 F., Jiang, J. H., Knosp, B. W., Stek, P. C., Wagner, P. A., and Wu, D. L.: *EOS MLS Version 3.3*
637 *Level 2 data quality and description document, Tech. rep., Jet Propulsion Laboratory*, available
638 at: <http://mls.jpl.nasa.gov/>), 2011.

639

640 McPeters, R. D., G. J. Labow, and J. A. Logan, Ozone climatological profiles for satellite
641 retrieval algorithms, *J. Geophys. Res.*, *112*, D05308, doi:10.1029/2005JD006823, 2007.

642

643 McPeters, R. D., and G. J. Labow, Climatology 2012: An MLS and sonde derived ozone
644 climatology for satellite retrieval algorithms, *J. Geophys. Res.*, *117*, doi:10.1029/2011JD017006,
645 2012.

646

647 McPeters, R. D., P. K. Bhartia, D. Haffner, G. J. Labow, and L. Flynn, The version 8.6 SBUV
648 ozone data record: An overview, *J. Geophys. Res.*, *118*, 8032–8039, doi:10.1002/jgrd.50597,
649 2013.

650

651 Molod, A., L. Takacs, M. Suarez, and J. Bacmeister, Development of the GEOS-5 atmospheric
652 general circulation model: evolution from MERRA to MERRA2, *Geosci. Mod. Dev.*, *8*,
653 doi:10.5194/gmd-8-1339-2015, 2015.

654
655 Oman, L. D., A. R. Douglass, J. R. Ziemke, J. M. Rodriguez, D. W. Waugh, and J. E. Nielsen,
656 The ozone response to ENSO in Aura satellite measurements and a chemistry-climate
657 simulation, *J. Geophys. Res.*, *118*, 965-976, doi:10.1029/2012JD018546, 2013.
658
659 Orbe, C., L. D. Oman, S. E. Strahan, D. W. Waugh, S. Pawson, L. L. Takacs, and A. M. Molod,
660 Large-Scale Atmospheric Transport in GEOS Replay Simulations, *J. Adv. Mod. Earth Sys.*, *9*,
661 2545-2560, 2017.
662
663 Park, J. H., M. K. Ko, C. H. Jackman, R. A. Plumb, J. A. Kaye, and K. H. Sage, Models and
664 Measurements Intercomparison II, *NASA Tech. Memo.*, *NASA/TM-1999-209554*, 502 pp., 1999.
665
666 Parrish, A., Boyd, I. S., Nedoluha, G. E., Bhartia, P. K., Frith, S. M., Kramarova, N. A., Connor,
667 B. J., Bodeker, G. E., Froidevaux, L., Shiotani, M., and Sakazaki, T.: Diurnal variations of strato-
668 spheric ozone measured by ground-based microwave remote sensing at the Mauna Loa NDACC
669 site: measurement validation and GEOSCCM model comparison, *Atmos. Chem. Phys.*, *14*, 7255-
670 7272, <https://doi.org/10.5194/acp-14-7255-2014>, 2014.
671
672 Richman, M. B., Rotation of principal components, *J. Clim.*, *6*, 293-335,
673 <https://doi.org/10.1002/joc.3370060305>, 1986.
674
675 Rodgers, C. D., Inverse methods for atmospheric sounding: theory and practice, *World Scientific*
676 *Publishing Co.*, pp. 238, London, United Kingdom, 2000.
677
678 Shepherd, T. G., D. A. Plummer, J. F. Scinocca, M. I. Hegglin, V. E. Fioletov, M. C. Reader, E.
679 Remsberg, T. von Clarmann, and H. J. Wang, Reconciliation of halogen-induced ozone loss with
680 the total-column ozone record, *Nature Geosci.*, *7*, doi:10.1038/NGEO2155, 2014.
681
682 Stanford, J. L., J. R. Ziemke, and S. Y. Gao, Stratospheric circulation features deduced from
683 SAMS constituent data, *J. Atmos. Sci.*, *50*, 226-246, 1993.
684

685 Stauffer, R. M., A. M. Thompson, L.D. Oman, and S.E. Strahan, The effects of a 1998 observing
686 system change on MERRA-2-based ozone profile simulations. *J. Geophys. Res. Atmos.*, *124*,
687 7429-7441, <https://doi.org/10.1029/2019JD030257>, 2019.

688
689 Strode, S. A., J. M. Rodriguez, J. A. Logan, O. R. Cooper, J. C. Witte, L. N. Lamsal, M. Damon,
690 B. Van Aartsen, S. D. Steenrod, and S. E. Strahan, Trends and variability in surface ozone over
691 the United States, *J. Geophys. Res. Atmos.*, *120*(17), 9020-9042, doi:10.1002/2014JD022784,
692 2015.

693
694 Strode, S. A., J. S. Wang, M. Manyin, B. N. Duncan, R. Hossain, C. A. Keller, S. E. Michel, and
695 J. W. C. White, Strong sensitivity of the isotopic composition of methane to the plausible range
696 of tropospheric chlorine, *Atmos. Chem. Phys.*, *20*, 8405–8419, [https://doi.org/10.5194/acp-20-](https://doi.org/10.5194/acp-20-8405-2020)
697 [8405-2020](https://doi.org/10.5194/acp-20-8405-2020), 2020.

698
699 Thompson, A. M., Witte, J. C., Sterling, C., Jordan, A., Johnson, B. J., Oltmans, S. J., Fujiwara,
700 M., Vömel, H., Allaart, M., Piters, A., Coetzee, G. J. R., Posny, F., Corrales, E., Andres Diaz, J.,
701 Félix, C., Komala, N., Lai, N., Maata, M., Mani, F., Zainal, Z., Ogino, S.-Y., Paredes, F., Luiz
702 Bezerra Penha, T., Raimundo da Silva, F., Sallons-Mitro, S., Selkirk, H. B., Schmidlin, F. J.,
703 Stuebi, R., and Thiongo, K.: First reprocessing of Southern Hemisphere Additional Ozonesondes
704 (SHADOZ) Ozone Profiles (1998–2016). 2. Comparisons with satellites and ground-based
705 instruments, *J. Geophys. Res.*, *122*, 13000–13025, <https://doi.org/10.1002/2017JD027406>, 2017.

706
707 Timmermans, R. M. A., R. F. van Oss, and H. M. Kelder, Equatorial Kelvin wave signatures in
708 ozone profile measurements from Global Ozone Monitoring Experiment (GOME), *J. Geophys.*
709 *Res.*, *110*, D21103, doi:10.1029/2005JD005929, 2005.

710
711 Wallace, J. M., R. L. Panetta, and J. Estberg, Representation of the equatorial stratospheric
712 Quasi-Biennial Oscillation in EOF phase space, *J. Atmos. Sci.*, *50*, 12, 1751-1762,
713 doi:10.1175/1520-0469(1993)050<1751:ROTESQ>2.0.CO;2, 1993.

714

715 Wargan, K., C. Orbe, S. Pawson, J. R. Ziemke, L. D. Oman, M. A. Olsen, et al., Recent decline
716 in extratropical lower stratospheric ozone attributed to circulation changes. *Geophys. Res. Lett.*,
717 *45*, 5166–5176. [https:// doi.org/10.1029/2018GL077406](https://doi.org/10.1029/2018GL077406), 2018.

718

719 Witte, J. C., Thompson, A. M., Smit, H. G. J., Fujiwara, M., Posny, F., Coetzee, G. J. R.,
720 Northam, E. T., Johnson, B. J., Sterling, C. W., Mohammed, M., Ogino, S.-Y., Jordan, A.,
721 daSilva, F. R., and Zainal, Z.: First reprocessing of Southern Hemisphere Additional
722 OZonesondes (SHADOZ) profile records (1998–2015) 1: Methodology and evaluation, *J.*
723 *Geophys. Res.*, *122*, 6611–6636, <https://doi.org/10.1002/2016JD026403>, 2017.

724

725 Ziemke, J. R., and J. L. Stanford, Quasi-biennial oscillation and tropical waves in total ozone, *J.*
726 *Geophys. Res.*, *99*, 23,041-23,056, 1994.

727 Ziemke, J. R., S. Chandra, A. Thompson, and D. McNamara, Zonal asymmetries in Southern
728 Hemisphere column ozone: Implications of biomass burning, *J. Geophys. Res.*, *101*, 14,421-
729 14,427, doi:10.1029/96JD01057, 1996.

730 Ziemke, J. R., S. Chandra, G. J. Labow, P. K. Bhartia, L. Froidevaux, and J. C. Witte, A global
731 climatology of tropospheric and stratospheric ozone derived from Aura OMI and MLS
732 measurements, *Atmos. Chem. Phys.*, *11*, 9237-9251, doi:10.5194/acp-11-9237-2011, 2011.

733

734 Ziemke, J. R., M. A. Olsen, J. C. Witte, A. R. Douglass, S. E. Strahan, K. Wargan, X. Liu, M. R.
735 Schoeberl, K Yang, T. B. Kaplan, S. Pawson, B. N. Duncan, P. A. Newman, P. K. Bhartia, M. K.
736 Heney, Assessment and applications of NASA ozone data products derived from Aura
737 OMI/MLS satellite measurements in context of the GMI Chemical Transport Model, *J. Geophys.*
738 *Res. Atmos.*, *119*, 5671-5699,doi:10.1002/2013JD020914, 2014.

739